Research Square

Preprints are preliminary reports that have not undergone peer review.
They should not be considered conclusive, used to inform clinical practice,
or referenced by the media as validated information.

Tibial cortex transverse transport promotes peripheral nerve regeneration in diabetic neuropathy through an NGF-dependent mechanism

Xingyu Chen
Guangxi Medical University
Feng Yang
Guangxi Medical University
Sijie Yang
The People's Hospital of Guangxi Zhuang Autonomous Region
Ruiqing Mo
Guangxi Medical University
Hongjie Su
Guangxi Medical University
Xi Yang
Guangxi University of Chinese Medicine
Feng Huang
Guangxi Medical University
Qikai Hua
hqk100@yeah.net
Guangxi Medical University

Article

Keywords: Tibial Cortex Transverse Transport, Diabetic Peripheral Neuropathy, NGF, Schwann cells, Mechanotransduction, Peripheral nerve regeneration

Posted Date: March 14th, 2026

DOI: https://doi.org/10.21203/rs.3.rs-8990113/v1

License: This work is licensed under a Creative Commons Attribution 4.0 International License.
Read Full License

Additional Declarations: No competing interests reported.

Abstract

Background

Diabetic peripheral neuropathy (DPN) causes progressive peripheral nerve dysfunction with limited recovery. Tibial cortex transverse transport (TTT) is an orthopedic mechanotherapy used in ischemic limb disorders, but its potential for peripheral nerve repair in DPN remains unclear.

Methods

DPN rats (high-fat diet plus low-dose streptozotocin) were assigned to Control, DPN, Sham, TTT, and TTT plus nerve growth factor (NGF) neutralization groups. Sensory behavior, gait-related function, motor/sensory nerve conduction, and histological outcomes were evaluated. In vitro, serum from each group was applied to Schwann cells, and a Schwann cell–dorsal root ganglion (DRG) neuron co-culture system was used to assess neurite outgrowth.

Results

TTT improved sensory function and gait performance, increased motor and sensory conduction velocities, and ameliorated structural abnormalities in sciatic nerve and intraepidermal nerve fibers. Sciatic nerve NGF showed a modest increase after TTT, and TTT-derived serum enhanced Schwann cell viability, increased NGF secretion, and promoted DRG neurite extension in vitro. NGF neutralization attenuated multiple TTT-associated benefits in vivo and in vitro.

Conclusions

TTT confers neurofunctional and structural benefits in experimental DPN, with NGF signaling contributing to its effects, supporting TTT as a promising mechanotherapy for peripheral nerve repair.

1. Introduction

Diabetic Peripheral Neuropathy (DPN) is a common and debilitating complication of diabetes, characterized by nerve damage that leads to sensory loss, pain, and an increased risk of diabetic foot ulcers [1, 2]. Despite significant advancements in treatment, most current therapies primarily focus on alleviating symptoms rather than addressing the underlying nerve degeneration, leaving a critical gap in effective treatments for nerve repair and regeneration [3]. This challenge arises from the complex pathophysiology of DPN, which includes factors such as hyperglycemia-induced nerve damage, impaired neurotrophic support, and inflammatory processes, making complete regeneration difficult to achieve [3, 4]. Conventional therapeutic approaches, including pharmacological interventions and physical therapies like electrical stimulation, have shown limited success in reversing nerve degeneration or stimulating

meaningful nerve regeneration [4–6][4–6]. While these therapies may offer temporary relief, they often fail to fully address the root causes of DPN, and the regeneration of peripheral nerves remains a major hurdle due to the difficulty in targeting the necessary repair mechanisms [7, 8].

Tibial Cortex Transverse Transport (TTT), a novel orthopedic technique originally developed for treating lower limb ischemic diseases, such as diabetic foot ulcers and peripheral artery disease, has emerged as a promising therapy for nerve regeneration [9–11]. TTT has been refined as a minimally invasive surgical technique using smaller incisions and external fixation-assisted tibial corticotomy [12]. TTT applies controlled mechanical strain through tibial bone distraction, creating a biologically active regenerative microenvironment rather than merely enhancing vascular perfusion. Recent experimental evidence demonstrates that TTT accelerates tissue repair and is accompanied by robust neovascularization and activation of angiogenesis-related signaling pathways, including HIF-1α/SDF-1/CXCR4, together with enhanced endothelial progenitor cell–associated responses [10, 13, 14]. These findings suggest that TTT induces an organized systemic/regional repair program rather than a purely descriptive “regenerative environment.”

Anecdotally, during routine clinical follow-up, we noted that some diabetic foot patients undergoing TTT appeared to show altered plantar sensory responses to light mechanical stimulation; however, these observations were not prospectively collected or quantitatively assessed. Emerging skeletal neurobiology also provides a conceptual framework for bidirectional bone–nerve communication: bone injury can engage somatosensory afferents, and sensory neuron–derived trophic signaling contributes to fracture repair [15]. Because TTT involves a controlled osteotomy/distraction stimulus, we reasoned that bone-derived mechanical cues might influence peripheral nerve function and neurotrophic support, providing a hypothesis-generating rationale to investigate neurotrophic mechanisms of TTT in DPN.

Peripheral nerve repair depends strongly on Schwann cell–mediated support programs, including the production of neurotrophic factors such as nerve growth factor (NGF) [16, 17]. NGF is a key regulator of axonal maintenance and regeneration and plays a critical role in sensory fiber survival and functional recovery in peripheral neuropathies such as DPN [18]. Importantly, mechanotransduction has emerged as an upstream regulator of Schwann cell biology; mechanical stimulation or stretching can directly alter Schwann cell signaling and metabolic states [19, 20]. This provides a biologically plausible link between TTT-derived mechanical cues and Schwann cell–dependent neurotrophic support. Given that NGF–TrkA signaling is closely associated with sensory fiber maintenance and load-induced tissue adaptation [21, 22], we hypothesize that TTT-derived mechanical stimulation promotes Schwann cell activation and enhances NGF–TrkA signaling, thereby contributing to functional recovery in DPN. To test this hypothesis, we evaluated the effects of TTT on Schwann cell activation and NGF-related neurotrophic support in a rat model of DPN and further examined whether neutralizing NGF attenuates the neuroprotective effects of TTT.

2. Materials and Methods

2.1 Cells and Animals

The RSC96 cells (rat Schwann cell line) were purchased from Wuhan Procell Life Science & Technology Co. Ltd. (Wuhan, China). The experimental animals were 8-week-old healthy male Sprague-Dawley (SD) rats, which were raised in an SPF-grade environment with free access to food and water. The experimental animals were obtained from the Animal Center of Guangxi Medical University. Our animal experiments have been approved by the Ethics Committee of Guangxi Medical University (Approval Number: 202508018).

2.2 In Vivo Experiment

2.2.1 Modelling, Grouping and Administration

30 male SD rats, aged 8 weeks and weighing 180–200 g, were randomly divided into two cohorts: a control group (n = 6) maintained on standard chow, and a modeling cohort (n = 24) subjected to DPN induction. The modeling cohort was initially administered low-dose Streptozotocin (STZ; Sigma-Aldrich, St. Louis, MO, USA) injections (20 mg/kg ip) for 3 consecutive days [23]. Following this, the modeling cohort was fed a high-fat, high-sucrose diet (67.5% regular chow, 10% lard, 20% sucrose, and 2.5% cholesterol) for 8 weeks to induce type 2 diabetes with associated DPN [24]. The control cohort received an equal volume of citrate buffer for 3 consecutive days and continued on standard chow throughout the experiment. Sustained blood glucose ≥ 16.7 mmol/L was used as the criterion for successful diabetes induction [25]. Eight weeks post-injection, behavioral tests were performed to evaluate peripheral nerve function and confirm the successful establishment of the DPN model [24].

Following validation, all 30 rats were allocated into five experimental groups (n = 6): (i) Control (untreated normoglycemic rats), (ii) DPN (diabetic rats with peripheral neuropathy), (iii) Sham (DPN rats receiving cortical osteotomy without bone transport), (iv) TTT (DPN rats undergoing a full tibial transverse transport protocol for 10 consecutive days), and (v) TTT+anti-NGF (DPN rats receiving anti-NGF treatment prior to TTT).

For Sham and TTT surgeries, a tibial cortical osteotomy window was created and a customized external fixator was applied to the operated limb; Sham rats underwent identical procedures except that no transport was performed. After a postoperative latency period, tibial transverse transport was carried out in the TTT groups for 10 consecutive days (outward transport followed by inward transport), and the cortical fragment was returned to its original position before tissue collection (Fig. 1). For the TTT+anti-NGF group, DPN rats were given a single subcutaneous injection of a neutralizing anti-rat β-NGF antibody (8 μg in 50 μL; R&D Systems, Minneapolis, MN, USA; No. AF-556-NA) immediately before TTT. The antibody is a full-length goat IgG, which typically exhibits an in vivo half-life of approximately 5–8 days in rodents due to FcRn-mediated recycling; therefore, a single injection was expected to provide sustained NGF neutralization during the 10-day TTT period. All surgical procedures were performed as previously described [26, 27]. On post-operative day 14, peripheral blood, sciatic nerves and plantar skin were harvested for downstream analyses (Fig. 1).

2.2.2 Behavioural Tests

Gait test and SFI. Hind-paw footprints were collected using a walking-track test from the right hind limb. Print length (PL; heel to the 3rd toe), toe spread (TS; 1st–5th toes), and intermediary toe spread (IT; 2nd–4th toes) were measured from ≥ 3 clear footprints per rat and averaged to obtain EPL, ETS, and EIT. The sciatic functional index (SFI) was calculated as: SFI =-38.3(EPL-NPL)/NPL + 109.5(ETS-NTS)/NTS + 13.3(EIT-NIT)/NIT-8.8. Because DPN is typically bilateral, “normal” reference values (NPL, NTS, NIT) were defined as the mean right-hind footprint parameters from age-matched non-diabetic Control group measured under identical conditions. One SFI value per animal was used for statistical analysis[28, 29].

Neurological function was evaluated on the 8th week after DPN modeling and the 14th day after TTT procedures [23, 30]. Mechanical pain threshold was assessed by adapting rats on a metal grid for 30 minutes, followed by incremental mechanical stimulation of the hind paw sole using an electronic Von Frey aesthesiometer (model 38450, Ugo Basile, Gemonio, Italy). Thermal pain threshold was measured using a 55°C hot plate analgesia meter (model 35100, Ugo Basile, Gemonio, Italy), recording the latency to paw withdrawal or licking. Each behavioral test was performed five times at 5-minute intervals, and the average of the last three measurements was used as the final value.

For electrophysiological analysis, motor nerve conduction velocity (MNCV) and sensory nerve conduction velocity (SNCV) were recorded under 2% pentobarbital anesthesia using an electrophysiological recording system (model REMI-800, RWD Life Science, Shenzhen, China). For MNCV measurement, the sciatic nerve was exposed and stimulated at the nerve bifurcation with a constant-current stimulator (model ISO-Flex, RWD Life Science, Shenzhen, China), while compound muscle action potential latency was recorded from the gastrocnemius muscle. For SNCV, the tibial nerve at the ankle was stimulated and the sensory nerve action potential latency was recorded from the distal sciatic nerve. Both MNCV and SNCV were calculated as: conduction velocity (m/s) = electrode spacing (mm) / latency (ms). All tests were conducted on the lower limb ipsilateral to the TTT surgery.

2.2.3 Histology

Sciatic nerve tissues, L4 dorsal root ganglia (DRGs), and hind paw epidermal skin samples were collected on post-operative day 14 and fixed overnight at 4°C in 4% paraformaldehyde. Tissues were dehydrated, embedded in paraffin, and sectioned at 5 μm. H&E staining was performed on sciatic nerve sections for general morphological evaluation. Nissl staining was performed on L4 DRG sections to assess neuronal somatic integrity and Nissl substance distribution. For semi-quantification, images were captured under identical microscope settings, and the number of Nissl-stained neurons was counted within a defined area (mm^2) in five random fields per section; values were averaged across fields/sections to yield one value per rat (n = 6 per group) for statistical analysis [31]. TUNEL staining was performed on sciatic nerve sections using a commercial kit (G1501, Servicebio, Wuhan, China). For TUNEL quantification, TUNEL-positive nuclei were defined as nuclei showing distinct green fluorescence co-localizing with DAPI, and the apoptotic index was calculated as (TUNEL-positive nuclei / total DAPI nuclei) × 100 using ImageJ (NIH, Bethesda, MD, USA). Immunohistochemistry for PGP9.5 was

conducted on hind paw epidermal skin sections using primary antibody PGP9.5 (1:1000, Proteintech, China) and a DAB chromogenic kit (Servicebio, Wuhan, China).

2.2.4 Western Blot

Total protein was extracted from sciatic nerve tissues and quantified using the BCA assay. Equal protein amounts were separated by SDS-PAGE and electrotransferred onto nitrocellulose membranes. Following blocking with 5% (w/v) skim milk in TBST for 2 h at room temperature, membranes were incubated overnight at 4°C with primary antibodies against NGF (1:1000, wanleibio, China) or β-actin (loading control, 1:10000, Proteintech, China) diluted in 3% BSA/TBST. The next day, blots were washed and probed with horseradish peroxidase-conjugated secondary antibodies (1:10000, Proteintech, China) for 2 h. Immunoreactive bands were visualized using ECL Western Blotting detection reagent (BL520A, Biosharp, China).

For western blotting, proteins from six rats per group were combined in equal amounts to generate one pooled sample per group (group-level average). The pooled samples were run on three independent blots as technical repeats, and densitometry values were averaged across blots for presentation. Because samples were pooled at the group level, the western blot data were used to assess technical repeat consistency and overall trends, rather than inferential statistics based on biological replicates. Full-length uncropped western blot images and membrane cutting/assembly information are provided (Figure S2).

2.3 In Vitro Experiment

2.3.1 Cell Culture

RSC96 cells were maintained in high-glucose DMEM medium with 10% FBS and 1% penicillin/streptomycin, and incubated at 37°C in a humidified 5% CO_2 atmosphere. For in vitro DPN model induction, cells were exposed to 200 mM glucose for 24 hours. RSC96 is a widely used rat Schwann cell line that retains key Schwann-cell features and is commonly employed to model diabetic peripheral nerve injury in vitro [32]. High-glucose exposure can trigger early stress/apoptosis-related responses in Schwann cells within 24 h; thus, we used a 24-h high-glucose challenge as an in vitro DPN-like injury paradigm [33].

DRG neurons were dissociated and cultured in accordance with established protocols [34, 35], with some modifications. In summary, the L4-L6 DRGs were extracted from adult SD rats, and the nerve roots were cut off. Then, the samples were transferred to a centrifuge tube containing an appropriate amount of collagenase NB 4G (Nordmark, 17465, Germany) and DNase (servivebio, G3342, China), with final concentrations of 0.5 mg/ml and 4 mg/ml, respectively. The samples were dissected with micro-scissors for 5 minutes and shaken at 37°C for 30min, followed by centrifugation to remove the collagenase and DNAase. Next, we added 0.25% trypsin (Gibco), and they were shaken at 37°C for 15min. Upon the completion of digestion, the supernatant was discarded after centrifugation. Then, the cell suspension was filtered through a 100-μm cell strainer to remove pieces of tissues. The neurons were resuspended in a high-glucose DMEM medium containing 10% FBS and 1% penicillin/streptomycin, followed by

repeated pipetting to form a single-cell suspension. Neurons were seeded into 24-well plates at a density of 2×10^5 cells per well, coated with 10mL/L Poly-D-lysine solution (G4031, servicebio, China) 1 day in advance, and then used for co-culture with RSC96 cells.

2.3.2 Cell proliferation assay

Cell viability was assessed using the CCK-8 (WST-8) assay (CCK-8 kit, MCE, Monmouth Junction, NJ, USA). Whole blood was collected by cardiac puncture at the time of tissue harvest [36]. Blood was collected into plain tubes and allowed to clot undisturbed at room temperature for 15–30 min [37]. The clot was removed by centrifugation at 3000 rpm for 15 min, and the resulting supernatant (serum) was carefully transferred into clean polypropylene tubes. During handling, samples were kept at 2–8°C. Serum was aliquoted (e.g., 0.5 mL per tube) and stored at − 80°C until use; repeated freeze–thaw cycles were avoided [15].

To select the working serum concentration for subsequent assays, a pilot dose–response optimization was performed. RSC96 cells were seeded into 96-well plates at a density of 4 × 10^3 cells/well and incubated with rat serum at 2.5%, 5%, 10%, or 15% for 3 days. Following treatment, 10 μL of CCK-8 reagent was added to each well and plates were incubated at 37°C for 2 h. Absorbance at 450 nm was measured using a microplate spectrophotometer (SpectraMax iD3, Molecular Devices, San Jose, CA, USA). The concentration that yielded the highest OD450 (maximal viability signal) at the endpoint (Day 3) was selected as the working concentration; accordingly, 5% serum was used for subsequent experiments (optimization data shown in Fig. 4A). To exclude a confounding contribution of serum-borne NGF/BDNF, NGF and BDNF levels were also measured directly in the donor sera by ELISA (Figure S1), and no significant differences were observed among groups.

Using the selected condition, RSC96 cells were treated for 3 days with individual rat serum samples from the five experimental groups (control, DPN, sham, TTT, and TTT + anti-NGF). For each group, serum from each rat was tested separately (n = 6 biological replicates per group). For each serum sample, CCK-8 was performed in three technical replicate wells, and technical wells were averaged to yield one value per animal for statistical analysis.

2.3.3 ELISA

After serum treatment, the culture supernatant from RSC96 cells was collected and clarified by brief centrifugation, and NGF levels were measured using an ELISA kit according to the manufacturer's instructions. ELISA measurements were performed in technical triplicates for each supernatant sample, and replicates were averaged to obtain one value per donor serum (n = 6 per group). To evaluate whether differences in NGF could originate from the donor sera themselves, NGF and BDNF levels were also measured directly in the donor sera by ELISA (NGF: ZC-37163; BDNF: ZC-37020, ZCBIO, China) (Figure S1).

2.3.4 Co-culture of RSC96 cells and DRG neurons

Serum from individual rats in the five experimental groups (control, DPN, sham, TTT, and TTT + anti-NGF) was diluted to 5% (v/v) in high-glucose DMEM supplemented with 1% penicillin/streptomycin and 200 mM D-glucose (Sigma-Aldrich, St. Louis, MO, USA), with this concentration selected based on preliminary CCK-8 proliferation assays.

For the pre-treatment phase, RSC96 cells were trypsinized and seeded into the upper chamber of 0.4-μm pore Transwell inserts (Thermo Fisher Scientific, Waltham, MA, USA) at a density of 1×10^5 cells per 200 μL, while serum-free medium was added to the lower chamber. The upper chambers were then treated with the respective serum-supplemented medium for 72 hours. Following treatment, inserts were washed three times with PBS (Servicebio, Wuhan, China) to remove residual serum, and the medium was replaced with serum-free DMEM.

DRG neurons were pre-cultured at a density of 1.5×10^5 cells per well in the lower chamber of 24-well plates until adherence. DRG neurons were maintained in B-27 Plus–supplemented neuronal culture medium (Thermo Fisher Scientific, Waltham, MA, USA, A3653401).To establish co-culture, these neuron-containing wells were washed three times with PBS, after which the Transwell inserts containing pre-treated RSC96 cells were transferred onto the DRG cultures. Both compartments were maintained in serum-free medium during the 72-hour co-culture period.

After co-culture, DRG neurons in the lower chamber were fixed with 4% paraformaldehyde (Servicebio, Wuhan, China) and immunostained with anti-β-tubulin III antibody (1:1000, Proteintech, Wuhan, China), a neuronal marker for peripheral sensory neurons, including DRG neurons [38]. Because RSC96 cells were confined to the upper Transwell insert (0.4-μm pore size), the pore size prevents cell migration and allows only soluble factor exchange; thus, imaging and quantification were performed exclusively on β-tubulin III–positive DRG neurons in the lower chamber. Morphological analysis was performed using ImageJ software to quantify neurite length and branch points. For each donor serum (n = 6 per group), 50 randomly selected β-tubulin III–positive neurons were analyzed and averaged to yield one value per donor for statistical analysis.

2.3.5 Statistical Analysis

All data are presented as mean ± SD unless otherwise specified. Normality was assessed using the Shapiro–Wilk test and homogeneity of variances using Levene's test. For comparisons among ≥ 3 groups, one-way ANOVA was performed followed by Tukey's multiple-comparisons test (all pairwise comparisons) or Dunnett's test (comparisons vs. a single control), as specified in the figure legends. For count-type outcomes such as neurite branch points, nonparametric testing was applied using the Kruskal–Wallis test with Dunn's multiple comparisons. Where applicable, multiple comparisons were restricted to a priori defined contrasts (e.g., DPN vs TTT and TTT vs TTT+anti-NGF for Fig. 5C). Exact two-sided P values are reported (except when $P < 0.0001$). Statistical analyses were performed using GraphPad Prism 10.0, with $P < 0.05$ considered significant.

3. Results

3.1 Establishment and Validation of the DPN Rat Model

8 weeks after the final STZ injection, the 24 rats in the modeling cohort all achieved sustained hyperglycaemia (≥ 16.7 mmol/L). Relative to the age-matched control cohort (n = 6), these animals exhibited clear signs of peripheral neuropathy: mechanical withdrawal threshold dropped to 5.12 ± 0.24 g versus 14.63 ± 0.63 g (P < 0.001), thermal withdrawal latency prolonged to 14.69 ± 0.49 s versus 4.55 ± 0.37 s (P < 0.001), and nerve conduction velocities were markedly slowed (MNCV: 20.88 ± 0.86 m/s; SNCV: 24.33 ± 0.95 m/s vs. 40.00 ± 2.76 m/s and 62.00 ± 3.46 m/s, respectively; P < 0.001) (Table 1). These data verify that type 2 diabetic rats with established DPN were successfully generated before subsequent randomisation into intervention groups.

Table 1

Validation of the diabetic peripheral neuropathy (DPN) rat model. After 8 weeks of high-fat/high-sugar diet combined with low-dose STZ injections, rats in the DPN cohort (n = 24) exhibited significantly elevated blood glucose, reduced mechanical pain threshold, prolonged thermal pain latency, and decreased motor and sensory nerve conduction velocities compared with normal control rats (n = 6). These results confirm successful DPN model establishment. Data are shown as Mean ± SD. ***P < 0.001 vs. Control.

Group	n	Blood glucose (mmol/L)	Mechanical pain threshold (g)	Thermal pain response time (s)	MNCV (m/s)	SNCV (m/s)
Control	6	6.52 ± 0.94	14.63 ± 0.63	4.55 ± 0.37	40.00 ± 2.76	62.00 ± 3.46
DPN	24	21.52 ± 0.82***	5.12 ± 0.24***	14.69 ± 0.49***	20.88 ± 0.86***	24.33 ± 0.95***

3.2 TTT Improves Nerve Function and Plantar Morphology in DPN Rats

To evaluate functional recovery after TTT, we quantified hindlimb gait performance using walking-track analysis and calculated the Sciatic Functional Index (SFI) from right hind-limb footprints. DPN rats exhibited a marked impairment in SFI compared with controls, whereas TTT significantly improved SFI; this improvement was attenuated by NGF neutralization (Fig. 2A). Representative plantar images of the right hind paw are shown for qualitative reference (Fig. 2B). Consistent with the footprint-based SFI components, the 2nd-4th interdigital spacing (corresponding to the IT parameter) appeared reduced in DPN and improved after TTT, with attenuation by anti-NGF (Fig. 2B).

Following successful DPN validation (Section 3.1) and randomization, behavioral assessments were performed again 2 weeks after the interventions to assess treatment effects (post-TTT). At this post-intervention assessment, sensory deficits remained evident in DPN rats, consistent with the model-validation findings. TTT treatment substantially reversed these deficits, increasing the mechanical threshold to 12.45 ± 0.78 g and reducing the thermal latency to 6.82 ± 0.51 s (both P < 0.001 vs. DPN).

NGF neutralization markedly attenuated these improvements (mechanical: 7.89 ± 0.55 g; thermal: 11.24 ± 0.68 s; both $P < 0.05$ vs. TTT), whereas sham surgery exerted no significant effect (Fig. 2C, D).

Electrophysiological recordings performed at the same post-intervention timepoint showed that TTT markedly improved motor and sensory nerve conduction, increasing MNCV and SNCV to 35.67 ± 2.12 m/s and 51.83 ± 2.94 m/s, respectively (both $P < 0.01$ vs. DPN). These benefits were significantly diminished by NGF blockade ($P < 0.01$ vs. TTT), while sham-operated animals again showed no detectable improvement (Fig. 2E, F).

Immunohistochemical staining of PGP9.5 in hind paw skin demonstrated a marked loss of intraepidermal nerve fibers (IENFs) in DPN rats ($P < 0.001$ vs. Control). TTT significantly increased IENF density ($P < 0.001$ vs. DPN), whereas NGF neutralization largely abolished this neuroregenerative effect ($P < 0.001$ vs. TTT), consistent with the behavioral and electrophysiological findings (Fig. 2G, H).

3.3 TTT Improves Sciatic Nerve Pathology and Upregulates NGF Expression

H&E staining revealed marked morphological abnormalities in sciatic nerves from DPN rats compared with controls, whereas TTT-treated rats showed an overall improvement in nerve morphology; these changes were attenuated by NGF neutralization (Fig. 3A). To assess neuronal somatic integrity, Nissl staining was performed on L4 dorsal root ganglia (DRGs) (Fig. 3B). DPN rats exhibited disrupted neuronal morphology with reduced Nissl substance. Semi-quantification further demonstrated a marked decrease in the density of Nissl-stained neurons (neurons/mm²) in the DPN group compared with controls ($P < 0.001$). TTT significantly restored Nissl-stained neuron density relative to DPN ($P < 0.001$), whereas NGF neutralization markedly blunted this restorative effect (TTT vs. TTT+anti-NGF, $P < 0.001$). Notably, Nissl-stained neuron density did not differ between the DPN and TTT+anti-NGF groups ($P = 0.38$), indicating that NGF signaling contributes to the TTT-associated improvement in DRG neuronal integrity (Fig. 3C). Western blotting of pooled sciatic nerve lysates showed a modest increase in NGF in the TTT group compared with DPN, which was reduced by anti-NGF treatment (Fig. 3D, E). In parallel, TUNEL staining indicated elevated apoptosis in DPN nerves, which was reduced by TTT and partially reversed by NGF neutralization (Fig. 3F, G.).

3.4 TTT-Derived Serum Enhances Schwann Cell Survival and NGF Secretion

Serum concentration optimization identified 5% as the optimal dose, with rat serum most robustly enhancing RSC96 Schwann cell viability(Fig. 4A). Employing this concentration, serum from TTT-treated rats significantly improved cell viability compared to DPN and sham groups ($P < 0.001$), an effect markedly attenuated by NGF neutralization (Fig. 4B). ELISA quantification of RSC96 culture supernatants revealed that TTT serum increased NGF secretion to 24.42 ± 1.93 pg/mL, representing a ~ 1.4-fold elevation over DPN serum (17.09 ± 2.09 pg/mL, $P < 0.01$). This effect was abolished by NGF

neutralization (16.58 ± 1.19 pg/mL, P < 0.01 vs. TTT) (Fig. 4C). To exclude a confounding contribution from serum-borne neurotrophins, NGF and BDNF were also measured directly in the donor sera and showed no significant differences among groups (Figure S1), supporting that the differences observed in Fig. 4C reflect changes in cell-derived NGF in response to the different sera. Consistent with these findings, TUNEL staining indicated that TTT serum significantly reduced apoptosis in RSC96 cells relative to DPN serum, whereas NGF neutralization largely abolished this protective effect (Fig. 4D, E).

3.5 Axonal Stimulation of DRG Neurons by Serum-Primed Schwann Cells

To elucidate the functional impact of serum-primed Schwann cells on neuronal regeneration, we employed a Transwell co-culture system in which RSC96 cells were pre-treated with donor sera in the upper insert (0.4-μm pore size) and primary DRG neurons were maintained in the lower chamber. This configuration permits exchange of soluble factors but prevents cell mixing across compartments; therefore, neurite analyses were performed exclusively on β-tubulin III–positive DRG neurons in the lower chamber (Fig. 5A.). DRG neurons co-cultured with TTT serum–primed Schwann cells exhibited enhanced outgrowth, with average neurite length increasing to 89.2 ± 29.8 μm (P = 0.05 vs. DPN; one-way ANOVA with Tukey's multiple comparisons) and branch points rising to 4.0 ± 1.0 per neuron (P = 0.04 vs. DPN; Dunn's test, a priori DPN vs. TTT) (Fig. 5B/C.). In contrast, DPN serum–primed cells supported only minimal neurite extension (44.1 ± 29.2 μm; 2.4 ± 0.7 branches). NGF blockade significantly attenuated the TTT effect, reducing neurite length to 38.8 ± 25.2 μm (P = 0.02 vs. TTT; one-way ANOVA with Tukey's multiple comparisons) and branch points to 2.4 ± 0.7 (P = 0.03 vs. TTT; Dunn's test, a priori TTT vs. TTT+anti-NGF) (Fig. 5B/C.). For quantification, each dot represents one serum donor rat (n = 6 per group), with one value per donor obtained by averaging measurements from 50 randomly selected β-tubulin III–positive neurons. These results demonstrate that TTT serum enhances Schwann cell–mediated neuronal regeneration through NGF-dependent mechanisms.

4. Discussion

The present study demonstrates that TTT alleviates DPN-associated deficits across behavioral, electrophysiological, histological, and in vitro readouts, consistent with prior work showing that mechanical stimulation can trigger repair-promoting biological responses [39–42]. Our data support an NGF-dependent contribution to these benefits, as NGF neutralization attenuated TTT-associated improvements. Although our in vitro assays show that TTT-derived serum cues enhance Schwann cell viability and NGF secretion and support DRG neurite outgrowth, in vivo NGF detection was performed using whole-nerve lysates and does not identify the cellular source; thus, Schwann-cell involvement should be interpreted as a plausible contributor rather than a definitive in vivo source of NGF.

In our model, rats with DPN displayed typical sensory impairment and slowed nerve conduction, confirming successful model establishment [43, 44]. TTT significantly improved pain thresholds, conduction velocities, and gait-related functional readouts (including SFI), and was associated with

partially restored epidermal nerve fiber markers in hind paw skin. The fact that these improvements were diminished by NGF neutralization supports an NGF-dependent contribution to TTT-associated neurofunctional recovery. These findings align with established knowledge that NGF is a key neurotrophin essential for peripheral nerve maintenance and repair [45–48].

Histological analyses further revealed that TTT improved sciatic nerve morphology, partially restored L4 DRG neuronal somatic integrity as assessed by Nissl staining, and reduced apoptosis. Because sensory neuron cell bodies reside in DRGs and contribute to sciatic nerve function, the L4 DRG Nissl findings provide complementary evidence that TTT mitigates DPN-associated neuronal injury, while NGF blockade blunts these protective effects[49–51].

Consistent with this, serum derived from TTT-treated rats enhanced Schwann cell viability, increased NGF secretion, and reduced apoptosis in vitro. Schwann cells are central regulators of peripheral nerve regeneration, providing trophic support and guiding axonal extension [52–54]. The ability of TTT-derived serum to augment Schwann cell function suggests that systemic factors released during TTT may create a more supportive neuroregenerative environment. This is further supported by the observation that Schwann cells pre-stimulated with TTT serum significantly promoted DRG neurite elongation and branching, effects again dependent on NGF.

Translationally, our serum-based assays model systemic cues associated with TTT but do not translate to a clinical “dose,” given the complex mixture of circulating factors. Although serum NGF/BDNF levels did not differ among groups by ELISA, the in vitro effects likely reflect cellular responses to a multifactorial serum milieu rather than circulating NGF elevation alone [22, 55].

The mechanistic underpinnings of these findings may be closely linked to mechanical stimulation principles described in the Ilizarov tension-stress law, whereby bone distraction at approximately 1 mm/day induces 2–10% cyclic microstrain beneath the periosteum [56, 57]. Finite-element analyses have shown that such strain propagates along periosteal and Haversian canal pathways to the neurovascular bundle, exposing adjacent nerves to low-amplitude, high-frequency tension signals [21, 57–60]. These mechanical cues likely alter the local microenvironment surrounding peripheral nerves, including changes in mechanical pressure, extracellular matrix composition, and local cytokine concentrations [61–64]. Such microenvironmental modulation may directly stimulate NGF expression within neural tissue through mechanotransduction pathways [21, 65, 66]. Mechanical forces have been shown in other contexts to activate transcriptional regulators, calcium channels, or MAPK-related pathways that promote neurotrophin upregulation [61, 63, 64, 67].

Once NGF increases locally, several downstream biological effects may contribute to nerve repair. First, NGF may act through autocrine or paracrine mechanisms on Schwann cells and neurons, enhancing their survival and functional recovery [33, 68–70]. Second, increased NGF can initiate a broader neurotrophic cascade, potentially elevating other growth factors such as BDNF or GDNF, thereby amplifying regenerative signaling [22, 71]. Third, NGF possesses well-described neuroprotective and anti-apoptotic properties, including activation of PI3K/Akt or MAPK/ERK pathways, which can shield neurons

from hyperglycemia-induced damage [33, 70]. Fourth, NGF facilitates axonal regeneration and remyelination, processes essential for restoring conduction velocity and sensory function [22, 69, 72]. These mechanisms align well with our observed improvements in nerve conduction, fiber morphology, and DRG neurite outgrowth.

Together, these findings support a working model in which TTT-induced mechanical strain modulates the peri-neural microenvironment and engages NGF-dependent neuroprotective signaling (Fig. 6). Increased NGF signaling may promote regeneration through coordinated actions on neurons and glia, including Schwann cells [22, 69, 72]. Given the lysate-based nature of the in vivo NGF measurement, this mechanism is presented as a hypothesis supported by functional NGF neutralization and Schwann cell–based in vitro responses.

Potential relevance to sympathetic/autonomic fibers. Although our study focuses on somatosensory recovery, NGF signaling is also relevant to sympathetic/autonomic axons and may influence autonomic components of DPN. Prior work indicates that NGF can be upregulated after injury and contribute to sympathetic axon growth/regeneration, and sympathetic fibers constitute a notable fraction of axons within the sciatic nerve [73–76]. Because we did not directly assess sympathetic regeneration (e.g., TH-positive fiber density) or autonomic function (e.g., sudomotor output) in the present study, the potential contribution of autonomic recovery remains to be defined in future work.

While the study provides compelling evidence for an NGF-mediated mechanism, several limitations should be noted. We did not directly evaluate autonomic outcomes (e.g., TH-positive fibers, sudomotor output), and NGF blockade was systemic rather than nerve-specific. Other neurotrophic factors may also contribute to TTT-induced neural repair and warrant further investigation [22, 77, 78]. Representative plantar images were provided for qualitative reference, whereas peripheral innervation changes were quantified using epidermal nerve fiber markers; additional parameter-wise scoring of paw morphology could further standardize gross morphological comparisons in future studies. H&E provides an overview of nerve morphology but is not ideal for resolving remyelination/demyelination; additional myelin/axon-sensitive readouts (e.g., semithin toluidine blue sections, axon caliber distributions) and analysis of a purely sensory nerve (e.g., saphenous nerve) would strengthen conclusions regarding sensory axonal degeneration/regeneration. TUNEL staining reports overall apoptosis but does not identify protected cell populations; future work should incorporate cell-type markers. All in vivo analyses were performed at day 14 post-intervention, capturing early recovery but not durability; longer follow-up is needed.

In vitro, an iso-osmotic control for high-glucose conditions (e.g., mannitol/mannose) was not included, and the use of an immortalized Schwann cell line improves reproducibility but does not fully recapitulate in vivo microenvironmental changes; future studies using primary Schwann cells would further strengthen mechanistic interpretation. Only male rats were used, consistent with prior TTT modeling practice; female cohorts were not included due to practical constraints in model establishment (e.g., anesthesia/surgical tolerance) and should be incorporated in future studies. Finally, the magnitude of the

NGF protein change in sciatic nerve was modest and, because western blotting used pooled samples with technical repeats, is presented descriptively rather than as biological replicate–based inference.

Overall, this study identifies TTT as a promising mechanotherapy capable of promoting peripheral nerve regeneration through NGF-dependent pathways. By clarifying the neurobiological processes involved, these findings may inform the development of novel mechanostimulation-based interventions for a wide range of nerve-related diseases.

5. Conclusion

TTT improved functional and structural outcomes in a rat model of diabetic peripheral neuropathy, as evidenced by better gait-related performance, higher mechanical thresholds, faster nerve conduction, reduced neuronal injury/apoptosis, and increased epidermal nerve fiber–related signals. In parallel, serum from TTT-treated animals enhanced Schwann cell viability, increased NGF secretion, and supported DRG neurite outgrowth in vitro. Importantly, neutralization of NGF attenuated multiple TTT-associated benefits, indicating that NGF signaling contributes to the neuroprotective effects of TTT. Collectively, these findings support TTT as a promising mechanotherapy that may promote peripheral nerve repair in diabetic neuropathy and warrant further studies to define the upstream mechanotransduction pathways, the cellular sources of neurotrophic support in vivo, and the durability and translational potential of this approach.

Declarations

Funding

The author(s) disclose receipt of the following financial support for the research, authorship, and/or publication of this article: the National Natural Science Foundation of China (No. 82260448); the Guangxi Natural Science Foundation (No. 2023JJD140126); the Guangxi Key Research and Development Plan (No. 2021AB11027); the Key Research and Development Plan of Qingxiu District, Nanning City (No. 2020053); and the Clinical Research Climbing Plan of the First Affiliated Hospital of Guangxi Medical University (No. YYZS2020010).

Conflicts of Interest

The authors declare that there are no conflicts of interest regarding the publication of this article.

Acknowledgements

The authors thank the experimental platform support provided by the First Affiliated Hospital of Guangxi Medical University. The authors also acknowledge the technical assistance of laboratory staff involved in animal care and histological analysis.

Author Contributions

Chen Xingyu and Hua Qikai conceived and designed the study.

Chen Xingyu, Yang Feng, and Mo Ruiqing performed the animal experiments.

Yang Sijie and Su Hongjie conducted the in vitro experiments and data acquisition.

Yang Xi and Huang Feng contributed to data analysis and interpretation.

Chen Xingyu drafted the manuscript.

Hua Qikai critically revised the manuscript and supervised the project.

All authors reviewed and approved the final manuscript.

References

1. Elafros, M.A., et al., *Towards prevention of diabetic peripheral neuropathy: clinical presentation, pathogenesis, and new treatments*. Lancet Neurology, 2022. 21(10): p. 922–936.https://doi.org/10.1016/S1474-4422(22)00188-0
2. Sloan, G., D. Selvarajah, and S. Tesfaye, *Pathogenesis, diagnosis and clinical management of diabetic sensorimotor peripheral neuropathy*. Nature Reviews Endocrinology, 2021. 17(7): p. 400–420.https://doi.org/10.1038/s41574-021-00496-z
3. Eid, S.A., et al., *New perspectives in diabetic neuropathy*. Neuron, 2023. 111(17): p. 2623–2641.https://doi.org/10.1016/j.neuron.2023.05.003
4. Dillon, B.R., L. Ang, and R. Pop-Busui, *Spectrum of Diabetic Neuropathy: New Insights in Diagnosis and Treatment*. Annual Review of Medicine, 2024. 75: p. 293–306.https://doi.org/10.1146/annurev-med-043021-033114
5. Handzlik, M.K., et al., *Insulin-regulated serine and lipid metabolism drive peripheral neuropathy*. Nature, 2023. 614(7946): p. 118-+.https://doi.org/10.1038/s41586-022-05637-6
6. Li, K.Z., et al., *How vitamins act as novel agents for ameliorating diabetic peripheral neuropathy: A comprehensive overview*. Ageing Research Reviews, 2023. 91: p. 17.https://doi.org/10.1016/j.arr.2023.102064
7. Hakim, S., et al., *Macrophages protect against sensory axon loss in peripheral neuropathy*. Nature, 2025. 640(8057): p. 30.https://doi.org/10.1038/s41586-024-08535-1
8. Yao, X.Y., et al., *Dysregulated mast cell activation induced by diabetic milieu exacerbates the progression of diabetic peripheral neuropathy in mice*. Nature Communications, 2025. 16(1): p. 17.https://doi.org/10.1038/s41467-025-59562-z
9. Yu, L., et al., *Tibial cortex transverse transport surgery improves wound healing in patients with severe type 2 DFUs by activating a systemic immune response: a cross-sectional study*. International Journal of Surgery, 2025. 111(1): p. 257–272.https://doi.org/10.1097/js9.0000000000001897

10. Xie, J., et al., *Bone transport induces the release of factors with multi-tissue regenerative potential for diabetic wound healing in rats and patients*. Cell Reports Medicine, 2024. 5(6): p. 25.https://doi.org/10.1016/j.xcrm.2024.101588
11. Nie, X.Y., et al., *Tibial cortex transverse transport facilitating healing in patients with recalcitrant non-diabetic leg ulcers*. Journal of Orthopaedic Translation, 2021. 27: p. 1–7.https://doi.org/10.1016/j.jot.2020.11.001
12. Li, G., et al., *How to perform minimally invasive tibial cortex transverse transport surgery*. Journal of Orthopaedic Translation, 2020. 25: p. 28–32.https://doi.org/10.1016/j.jot.2020.06.005
13. Wang, M., et al., *Transcriptomic analysis of bone transport reveals different functions between both ends*. Front Physiol, 2025. 16: p. 1592288.https://doi.org/10.3389/fphys.2025.1592288
14. Qin, W., et al., *Tibial cortex transverse transport promotes ischemic diabetic foot ulcer healing via enhanced angiogenesis and inflammation modulation in a novel rat model*. 2024. 29(1): p. 155
15. Xu, M., et al., *Mapping somatosensory afferent circuitry to bone identifies neurotrophic signals required for fracture healing*. 2026. 391(6781): p. eadr9608
16. Sundaram, V.K., et al., *Adipo-glial signaling mediates metabolic adaptation in peripheral nerve regeneration*. Cell Metabolism, 2023. 35(12): p. 27.https://doi.org/10.1016/j.cmet.2023.10.017
17. Huang, J.L., et al., *Neurophilic Biomimetic Lipoprotein-Mediated Targeted Nerve Growth Factor Delivery for Traumatic Brain Injury Therapy*. Advanced Science, 2025: p. 19.https://doi.org/10.1002/advs.202509405
18. Blaszkiewicz, M., et al., *Gene therapy approaches for obesity-induced adipose neuropathy: Device-targeted AAV-mediated neurotrophic factor delivery to adipocytes in subcutaneous adipose*. Molecular Therapy, 2024. 32(5): p. 1407–1424.https://doi.org/10.1016/j.ymthe.2024.02.035
19. Shan, F., et al., *Mechanosensitive channel of large conductance enhances the mechanical stretching-induced upregulation of glycolysis and oxidative metabolism in Schwann cells*. 2024. 22(1): p. 93
20. Acheta, J., et al., *Piezo channels contribute to the regulation of myelination in Schwann cells*. Glia, 2022. 70(12): p. 2276–2289.https://doi.org/10.1002/glia.24251
21. Tomlinson, R.E., et al., *NGF-TrkA signaling in sensory nerves is required for skeletal adaptation to mechanical loads in mice*. Proceedings of the National Academy of Sciences of the United States of America, 2017. 114(18): p. E3632-E3641.https://doi.org/10.1073/pnas.1701054114
22. Li, R., et al., *Growth factors-based therapeutic strategies and their underlying signaling mechanisms for peripheral nerve regeneration*. Acta Pharmacologica Sinica, 2020. 41(10): p. 1289–1300.https://doi.org/10.1038/s41401-019-0338-1
23. Hossain, M.J., et al., *Peripheral Neuropathy Phenotyping in Rat Models of Type 2 Diabetes Mellitus: Evaluating Uptake of the Neurodiab Guidelines and Identifying Future Directions*. Diabetes & Metabolism Journal, 2022. 46(2): p. 198–221.https://doi.org/10.4093/dmj.2021.0347
24. Racine, K.C., et al., *The high-fat diet and low-dose streptozotocin type-2 diabetes model induces hyperinsulinemia and insulin resistance in male but not female C57BL/6J mice*. Nutrition Research, 2024. 131: p. 135–146.https://doi.org/10.1016/j.nutres.2024.09.008

25. Coppey, L.J., et al., *Determination of peripheral neuropathy in high-fat diet fed low-dose streptozotocin-treated female C57Bl/6J mice and Sprague-Dawley rats*. Journal of Diabetes Investigation, 2018. 9(5): p. 1033–1040.https://doi.org/10.1111/jdi.12814
26. Qin, W.C., et al., *Tibial cortex transverse transport promotes ischemic diabetic foot ulcer healing via enhanced angiogenesis and inflammation modulation in a novel rat model*. European Journal of Medical Research, 2024. 29(1): p. 13.https://doi.org/10.1186/s40001-024-01752-4
27. Liu, J., et al., *Tibial Cortex Transverse Transport Facilitates Severe Diabetic Foot Wound Healing via HIF-1α-Induced Angiogenesis*. Journal of Inflammation Research, 2024. 17: p. 2681–2696.https://doi.org/10.2147/jir.S456590
28. de Medinaceli, L., W.J. Freed, and R.J. Wyatt, *An index of the functional condition of rat sciatic nerve based on measurements made from walking tracks*. Experimental neurology, 1982. 77(3): p. 634 – 43.https://doi.org/10.1016/0014-4886(82)90234-5
29. Mehta, B.K., D. Nerkar, and S. Banerjee, *Characterization of Peripheral Neuropathy in Rat Model of Type 2 Diabetes*. Indian Journal of Pharmaceutical Education and Research, 2017. 51(1): p. 92–101.https://doi.org/10.5530/ijper.51.1.13
30. Hai, Q.S., et al., *Plantamajoside Promotes NGF/TrkA Pathway to Inhibit Neuronal Apoptosis and Improve Diabetic Peripheral Neuropathy*. Journal of Cellular and Molecular Medicine, 2025. 29(8): p. 16.https://doi.org/10.1111/jcmm.70571
31. Li, Y., et al., *Oral pyruvate effects on dorsal root ganglia in simulated weightlessness rats*. 2022. 12(1): p. 9–20
32. Zhang, H., et al., *Calcitriol prevents peripheral RSC96 Schwann neural cells from high glucose & methylglyoxal-induced injury through restoration of CBS/H < sub>*2%3C/sub %3E S *expression.* Neurochemistry International, 2016. 92: p. 49–57.https://doi.org/10.1016/j.neuint.2015.12.005
33. Li, R., et al., *NGF Attenuates High Glucose-Induced ER Stress, Preventing Schwann Cell Apoptosis by Activating the PI3K/Akt/GSK3β and ERK1/2 Pathways*. Neurochemical Research, 2017. 42(11): p. 3005–3018.https://doi.org/10.1007/s11064-017-2333-6
34. Wang, R., et al., *A combined protocol for isolation, culture, and patch-clamp recording of dorsal root ganglion neurons*. Biophysics reports, 2025. 11(2): p. 87–95.https://doi.org/10.52601/bpr.2024.240036
35. Perner, C. and C.L. Sokol, *Protocol for dissection and culture of murine dorsal root ganglia neurons to study neuropeptide release*. STAR protocols, 2021. 2(1): p. 100333.https://doi.org/10.1016/j.xpro.2021.100333
36. Beeton, C., A. Garcia, and K.G. Chandy, *Drawing blood from rats through the saphenous vein and by cardiac puncture*. Journal of visualized experiments: JoVE, 2007(7): p. 266.https://doi.org/10.3791/266
37. Yin, P.Y., et al., *Preanalytical Aspects and Sample Quality Assessment in Metabolomics Studies of Human Blood*. Clinical Chemistry, 2013. 59(5): p. 833–845.https://doi.org/10.1373/clinchem.2012.199257

38. Moskowitz, P.F. and M.M. Oblinger, *Sensory neurons selectively upregulate synthesis and transport of the beta III-tubulin protein during axonal regeneration*. The Journal of neuroscience: the official journal of the Society for Neuroscience, 1995. 15(2): p. 1545–55
39. Di, X.P., et al., *Cellular mechanotransduction in health and diseases: from molecular mechanism to therapeutic targets*. Signal Transduction and Targeted Therapy, 2023. 8(1).https://doi.org/10.1038/s41392-023-01501-9
40. Shou, Y.F., et al., *Mechano-Activated Cell Therapy for Accelerated Diabetic Wound Healing*. Advanced Materials, 2023. 35(47).https://doi.org/10.1002/adma.202304638
41. Vahidi, M., A.S. Rizkalla, and K. Mequanint, *Extracellular Matrix-Surrogate Advanced Functional Composite Biomaterials for Tissue Repair and Regeneration*. Advanced Healthcare Materials, 2024. 13(27).https://doi.org/10.1002/adhm.202401218
42. Xie, J., et al., *Bone transport induces the release of factors with multi-tissue regenerative potential for diabetic wound healing in rats and patients*. Cell Reports Medicine, 2024. 5(6).https://doi.org/10.1016/j.xcrm.2024.101588
43. Wu, B.R., Z.Y. Niu, and F. Hu, *Study on Risk Factors of Peripheral Neuropathy in Type 2 Diabetes Mellitus and Establishment of Prediction Model*. Diabetes & Metabolism Journal, 2021. 45(4): p. 526–538.https://doi.org/10.4093/dmj.2020.0100
44. Fan, B.Y., et al., *Mesenchymal stromal cell-derived exosomes ameliorate peripheral neuropathy in a mouse model of diabetes*. Diabetologia, 2020. 63(2): p. 431–443.https://doi.org/10.1007/s00125-019-05043-0
45. Su, H.T., et al., *A self-assembling peptide-based hydrogel containing NF- κ B inhibitors and NGF for peripheral nerve injury repair*. Biofabrication, 2025. 17(2).https://doi.org/10.1088/1758-5090/adc340
46. Zeng, W., et al., *TPP ionically cross-linked chitosan/PLGA microspheres for the delivery of NGF for peripheral nerve system repair*. Carbohydrate Polymers, 2021. 258.https://doi.org/10.1016/j.carbpol.2021.117684
47. Song, W.M., et al., *Unidirectional and sustainable release of NGF and BDNF from a chitosan gel-mediated multilayer ordered composite membrane in promoting both spinal cord and sciatic nerve injury repair*. International Journal of Biological Macromolecules, 2025. 290.https://doi.org/10.1016/j.ijbiomac.2024.138927
48. Liu, X., et al., *Effects of NGF-chitosan on alleviating secondary degeneration and repairing primary degeneration after expanded partial optic nerve transection*. Science China-Life Sciences, 2025. 68(8): p. 2393–2407.https://doi.org/10.1007/s11427-024-2756-9
49. Selvarajah, D., et al., *Diabetic peripheral neuropathy: advances in diagnosis and strategies for screening and early intervention*. Lancet Diabetes & Endocrinology, 2019. 7(12): p. 938–948.https://doi.org/10.1016/s2213-8587(19)30081-6
50. Yang, K., et al., *Progress in the treatment of diabetic peripheral neuropathy*. Biomedicine & Pharmacotherapy, 2022. 148.https://doi.org/10.1016/j.biopha.2022.112717

51. Brask-Thomsen, P.K., et al., *Development and Progression of Polyneuropathy Over 5 Years in Patients With Type 2 Diabetes*. Neurology, 2024. 103(3).https://doi.org/10.1212/wnl.0000000000209652
52. Bosch-Queralt, M., R. Fledrich, and R.M. Stassart, *Schwann cell functions in peripheral nerve development and repair*. Neurobiology of Disease, 2023. 176.https://doi.org/10.1016/j.nbd.2022.105952
53. Abdo, H., et al., *Specialized cutaneous Schwann cells initiate pain sensation*. Science, 2019. 365(6454): p. 695-+.https://doi.org/10.1126/science.aax6452
54. Salzer, J., M.L. Feltri, and C. Jacob, *Schwann Cell Development and Myelination*. Cold Spring Harbor Perspectives in Biology, 2024. 16(9).https://doi.org/10.1101/cshperspect.a041360
55. Apfel, S.C., et al., *Efficacy and safety of recombinant human nerve growth factor in patients with diabetic polyneuropathy - A randomized controled trial*. Jama-Journal of the American Medical Association, 2000. 284(17): p. 2215–2221.https://doi.org/10.1001/jama.284.17.2215
56. Ilizarov, G.A., *The tension-stress effect on the genesis and growth of tissues: Part II. The influence of the rate and frequency of distraction*. Clinical orthopaedics and related research, 1989(239): p. 263–85
57. Isaksson, H., et al., *Bone regeneration during distraction osteogenesis: Mechano-regulation by shear strain and fluid velocity*. Journal of Biomechanics, 2007. 40(9): p. 2002–2011.https://doi.org/10.1016/j.jbiomech.2006.09.028
58. Yin, D.G., B. Chen, and S.Y. Lin, *Finite element analysis on multi-toughening mechanism of microstructure of osteon*. Journal of the Mechanical Behavior of Biomedical Materials, 2021. 117.https://doi.org/10.1016/j.jmbbm.2021.104408
59. Zhen, P.X., et al., *Finite element analysis of biomechanical effects in rat tibia during tibial cortex transverse transport*. Frontiers in Bioengineering and Biotechnology, 2025. 13.https://doi.org/10.3389/fbioe.2025.1670040
60. Su, H., et al., *Finite element analysis safety of tibial cortex transverse transport*. Bone & Joint Research, 2025. 14(4): p. 281–291.https://doi.org/10.1302/2046-3758.144.Bjr-2024-0157.R1
61. Kong, L.C., et al., *Biomechanical microenvironment in peripheral nerve regeneration: from pathophysiological understanding to tissue*. Theranostics, 2022. 12(11): p. 4993–5014.https://doi.org/10.7150/thno.74571
62. Metafune, M., et al., *The extracellular matrix in peripheral nerve repair and regeneration: a narrative review of its role and therapeutic potential*. Frontiers in Neuroanatomy, 2025. 19.https://doi.org/10.3389/fnana.2025.1628081
63. Manganas, P., et al., *The role of mechanobiology on the Schwann cell response: A tissue engineering perspective*. Frontiers in Cellular Neuroscience, 2022. 16.https://doi.org/10.3389/fncel.2022.948454
64. Xu, Z.Y., J.A. Orkwis, and G.M. Harris, *Cell Shape and Matrix Stiffness Impact Schwann Cell Plasticity via YAP/TAZ and Rho GTPases*. International Journal of Molecular Sciences, 2021. 22(9).https://doi.org/10.3390/ijms22094821

65. Zhang, L., et al., *Cyclic mechanical stress modulates neurotrophic and myelinating gene expression of Schwann cells*. Cell Proliferation, 2015. 48(1): p. 59–66.https://doi.org/10.1111/cpr.12151
66. Rana, O.R., et al., *Mechanical stretch induces nerve sprouting in rat sympathetic neurocytes*. Autonomic Neuroscience-Basic & Clinical, 2010. 155(1–2): p. 25–32.https://doi.org/10.1016/j.autneu.2010.01.003
67. Mao, R.Y., et al., *Piezoelectric stimulation from electrospun composite nanofibers for rapid peripheral nerve regeneration*. Nano Energy, 2022. 98.https://doi.org/10.1016/j.nanoen.2022.107322
68. Huang, H.T., et al., *PI3K/Akt and ERK/MAPK Signaling Promote Different Aspects of Neuron Survival and Axonal Regrowth Following Rat Facial Nerve Axotomy*. Neurochemical Research, 2017. 42(12): p. 3515–3524.https://doi.org/10.1007/s11064-017-2399-1
69. Li, R., et al., *Nerve growth factor activates autophagy in Schwann cells to enhance myelin debris clearance and to expedite nerve regeneration*. Theranostics, 2020. 10(4): p. 1649–1677.https://doi.org/10.7150/thno.40919
70. Gu, C.L., et al., *Exploring the cellular and molecular basis of nerve growth factor in cerebral ischemia recovery*. Neuroscience, 2025. 566: p. 190–197.https://doi.org/10.1016/j.neuroscience.2024.12.049
71. Nicoletti, V.G., et al., *The Role of Metals in the Neuroregenerative Action of BDNF, GDNF, NGF and Other Neurotrophic Factors*. Biomolecules, 2022. 12(8).https://doi.org/10.3390/biom12081015
72. Wan, T., et al., *Growth factors: Bioactive macromolecular drugs for peripheral nerve injury treatment - Molecular mechanisms and delivery platforms*. Biomedicine & Pharmacotherapy, 2024. 170: p. 1–15.https://doi.org/10.1016/j.biopha.2023.116024
73. Pius-Sadowska, E. and B. Machalinski, *Pleiotropic activity of nerve growth factor in regulating cardiac functions and counteracting pathogenesis*. Esc Heart Failure, 2021. 8(2): p. 974–987.https://doi.org/10.1002/ehf2.13138
74. Schmalbruch, H., *Fiber composition of the rat sciatic nerve*. The Anatomical record, 1986. 215(1): p. 71–81.https://doi.org/10.1002/ar.1092150111
75. Tian, T., et al., *A Perspective on Electrical Stimulation and Sympathetic Regeneration in Peripheral Nerve Injuries*. Neurotrauma reports, 2024. 5(1): p. 172–180.https://doi.org/10.1089/neur.2023.0133
76. Liu, Y., et al., *Sensory and autonomic function and structure in footpads of a diabetic mouse model*. Scientific Reports, 2017. 7.https://doi.org/10.1038/srep41401
77. Grosu-Bularda, A., et al., *Optimizing Peripheral Nerve Regeneration: Surgical Techniques, Biomolecular and Regenerative Strategies-A Narrative Review*. International Journal of Molecular Sciences, 2025. 26(8).https://doi.org/10.3390/ijms26083895
78. Ye, Z.Q., et al., *Role of Transforming Growth Factor Beta in Peripheral Nerve Regeneration: Cellular and Molecular Mechanisms*. Frontiers in Neuroscience, 2022. 16.https://doi.org/10.3389/fnins.2022.917587

Figures

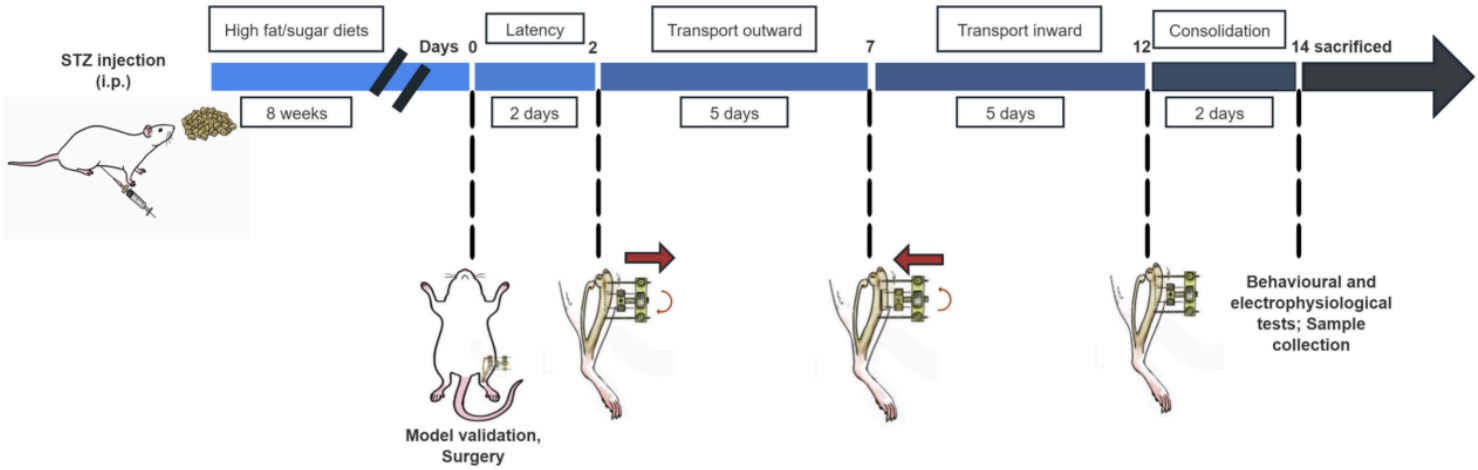


Figure 1

Experimental timeline, grouping strategy, and tibial transverse transport (TTT) procedure. After 8 weeks of high-fat/high-sugar diet combined with low-dose STZ injections, diabetic peripheral neuropathy (DPN) rats were randomly assigned to the DPN, Sham, TTT, and TTT+anti-NGF groups (n = 24 in total). Normal rats served as the Control group (n = 6). The schematic illustrates DPN induction, surgical preparation, latency (days 0–2), outward transport (days 2–7), inward transport (days 7–12), consolidation, and final behavioral/electrophysiological assessments and tissue collection on day 14. Sham rats underwent cortical osteotomy without transport. TTT rats received full tibial transverse transport, and TTT+anti-NGF rats received anti-NGF treatment prior to TTT.

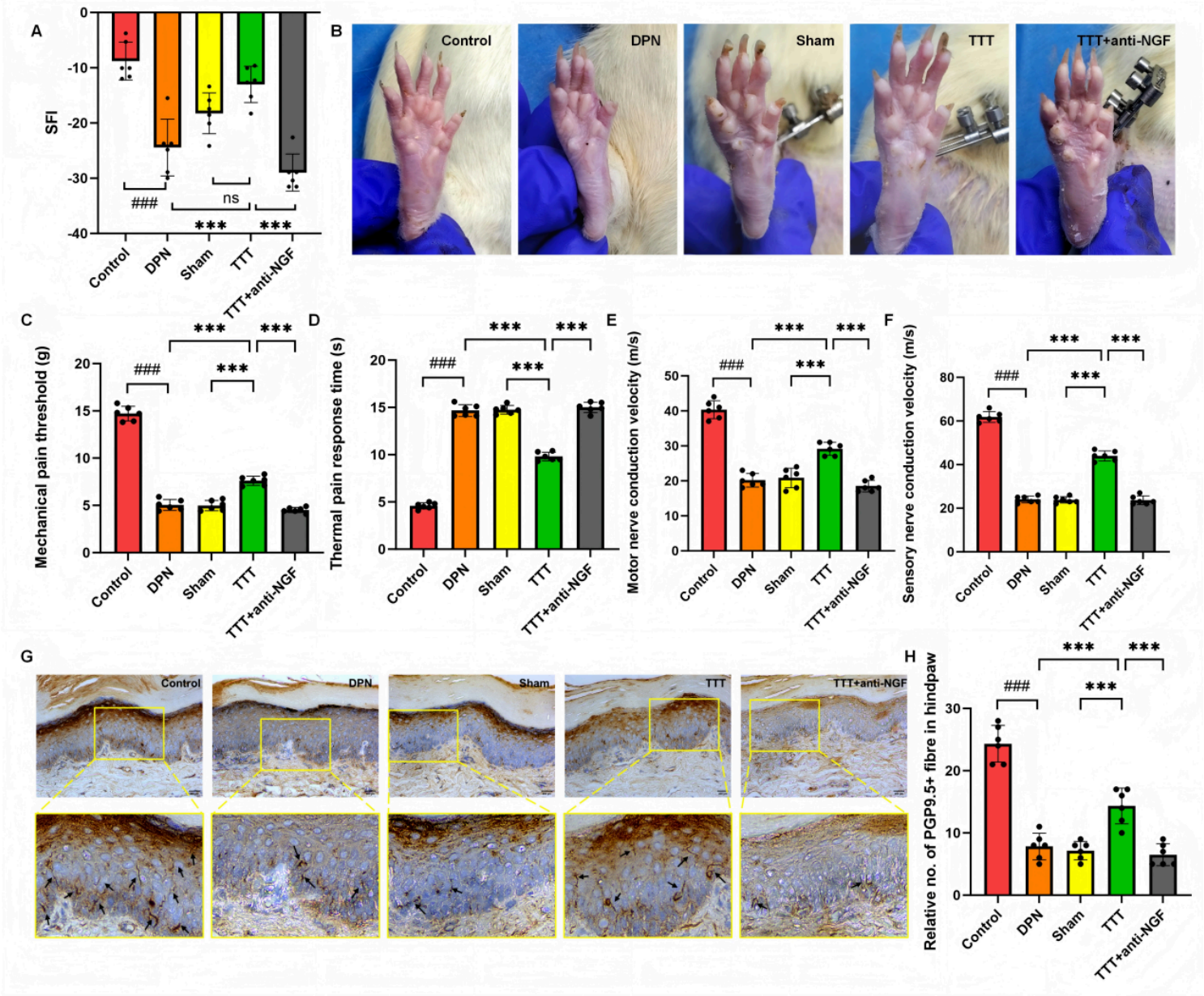


Figure 2

TTT improves behavioral sensitivity, nerve conduction, and cutaneous nerve integrity in DPN rats. (A) Sciatic Functional Index (SFI) of the right hind limb calculated from walking-track footprints. (B) Representative plantar images of the right hind paw. Qualitatively, the 2nd–4th interdigital spacing (corresponding to the IT parameter used in SFI) appeared reduced in DPN and improved after TTT, with attenuation by anti-NGF. (C) Mechanical pain threshold and (D) thermal withdrawal latency. (E) Motor nerve conduction velocity (MNCV) and (F) sensory nerve conduction velocity (SNCV). (G) Representative PGP9.5 immunohistochemical staining of intraepidermal nerve fibers (IENFs) in hind paw skin; scale bar = 50 μm. (H) Quantification of IENF density. Data are presented as Mean ± SD (n = 6). ###P < 0.001 vs. Control;***P < 0.001 vs. TTT; Tukey's multiple comparison test.

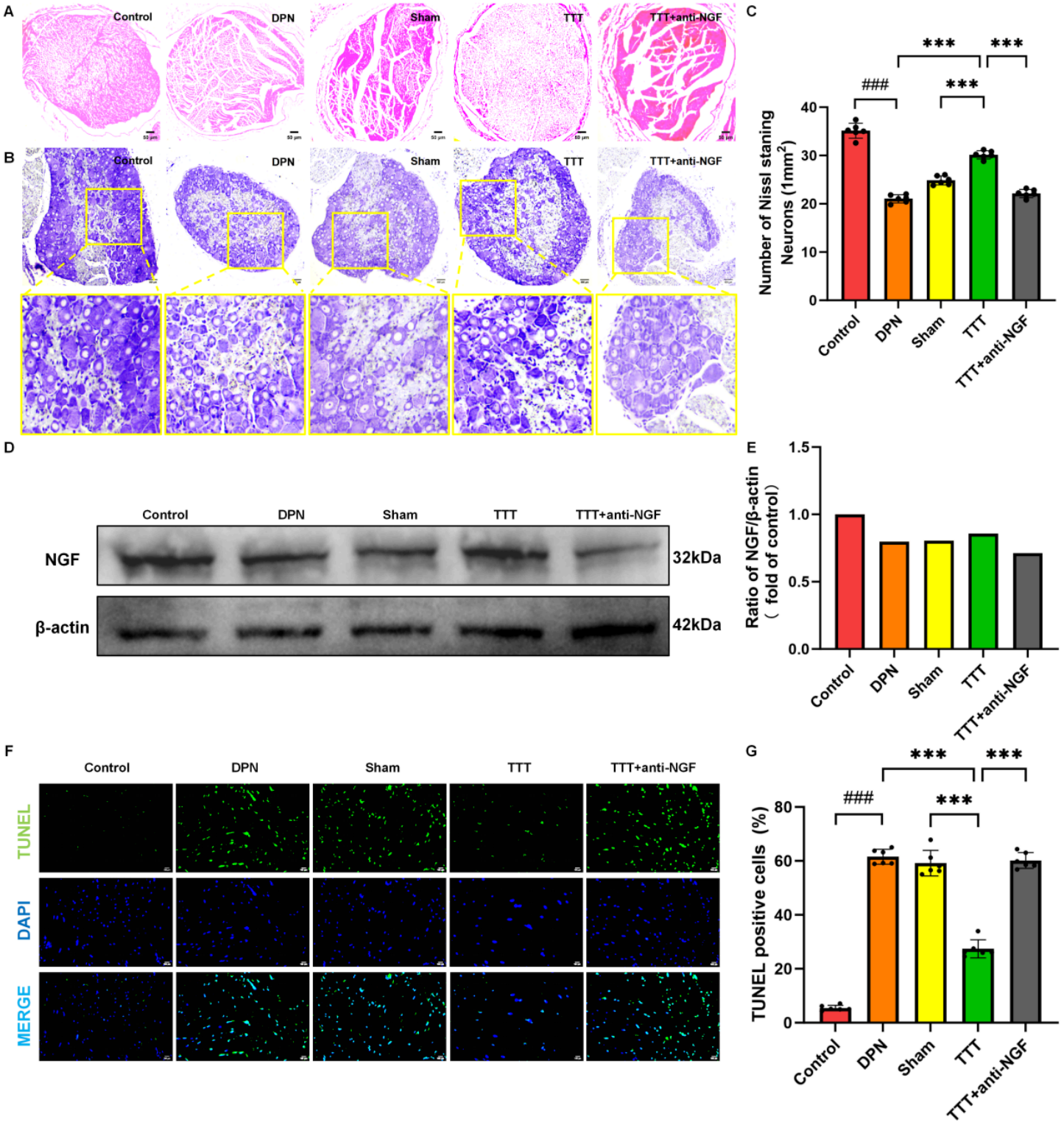


Figure 3

TTT alleviates sciatic nerve pathology and increases NGF expression in DPN rats. (A) Representative H&E staining of sciatic nerve sections showing overall nerve morphology (scale bar = 50 μm). (B) Representative Nissl staining of L4 dorsal root ganglia (DRGs) with corresponding higher-magnification insets (scale bars as indicated). (C) Semi-quantification of Nissl-stained neuron density (neurons/mm²) in L4 DRGs (n = 6 per group; one value per rat, averaged from five random fields per section). (D)

Representative western blots of NGF and β-actin in sciatic nerve lysates. (E) Densitometric quantification of NGF normalized to β-actin from three technical repeats (three independent blots) of pooled group samples (each lane represents one pooled sample per group). (F) Representative TUNEL staining (green) with DAPI counterstain (blue) in sciatic nerve sections (scale bar = 50 μm). (G) Quantification of TUNEL-positive cells (apoptotic index; n = 6 per group). Data are shown as mean ± SD. ###P < 0.001 vs. Control; *P < 0.05, **P < 0.01, ***P < 0.001 vs. TTT. For panels C and G, one-way ANOVA with Tukey's multiple comparisons was used. Panel E shows technical repeat consistency of pooled samples and is presented descriptively (no biological replicate–based inferential statistics).

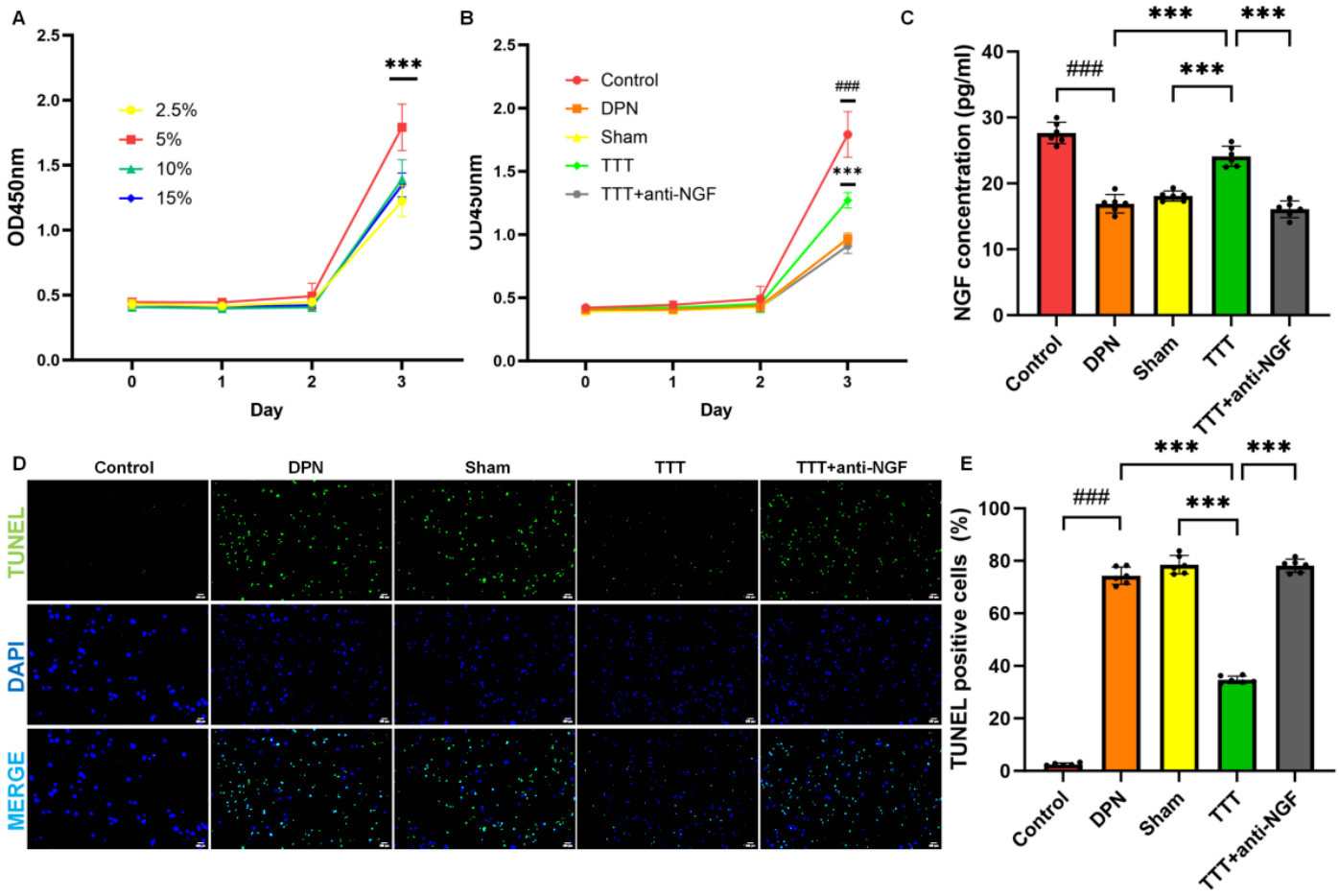


Figure 4

Serum from TTT-treated rats enhances Schwann cell viability, stimulates NGF secretion, and reduces apoptosis in vitro. (A) Time-course CCK-8 viability (OD450) across serum concentrations (2.5%, 5%, 10%, 15%). Statistics: two-way ANOVA (factors: time and concentration) with multiple-comparisons correction. (B) Schwann cell viability after 72-hour treatment with 5% serum from each experimental group (n = 6 serum donors per group; one value per donor). (C) NGF concentration in RSC96 culture supernatants measured by ELISA (n = 6 serum donors per group; one value per donor; technical triplicates averaged). To assess potential confounding by serum-borne neurotrophins, NGF and BDNF levels were also measured directly in donor sera and showed no significant differences among groups (Figure S1). (D) Representative TUNEL staining (green) with DAPI counterstain (blue) of RSC96 cells after

serum treatment (scale bar = 200 μm). TUNEL-positive nuclei were defined as green signals co-localizing with DAPI above a fixed threshold. (E) Quantification of TUNEL-positive cells (apoptotic index; n = 6 serum donors per group; one value per donor). Data are shown as mean ± SD. ###P < 0.001 vs. Control; *P < 0.05, **P < 0.01, ***P < 0.001 vs. TTT. For serum-based assays, n indicates the number of serum donor rats (n = 6 per group). For CCK-8, each donor serum was measured in three technical replicate wells, which were averaged to yield one value per donor.

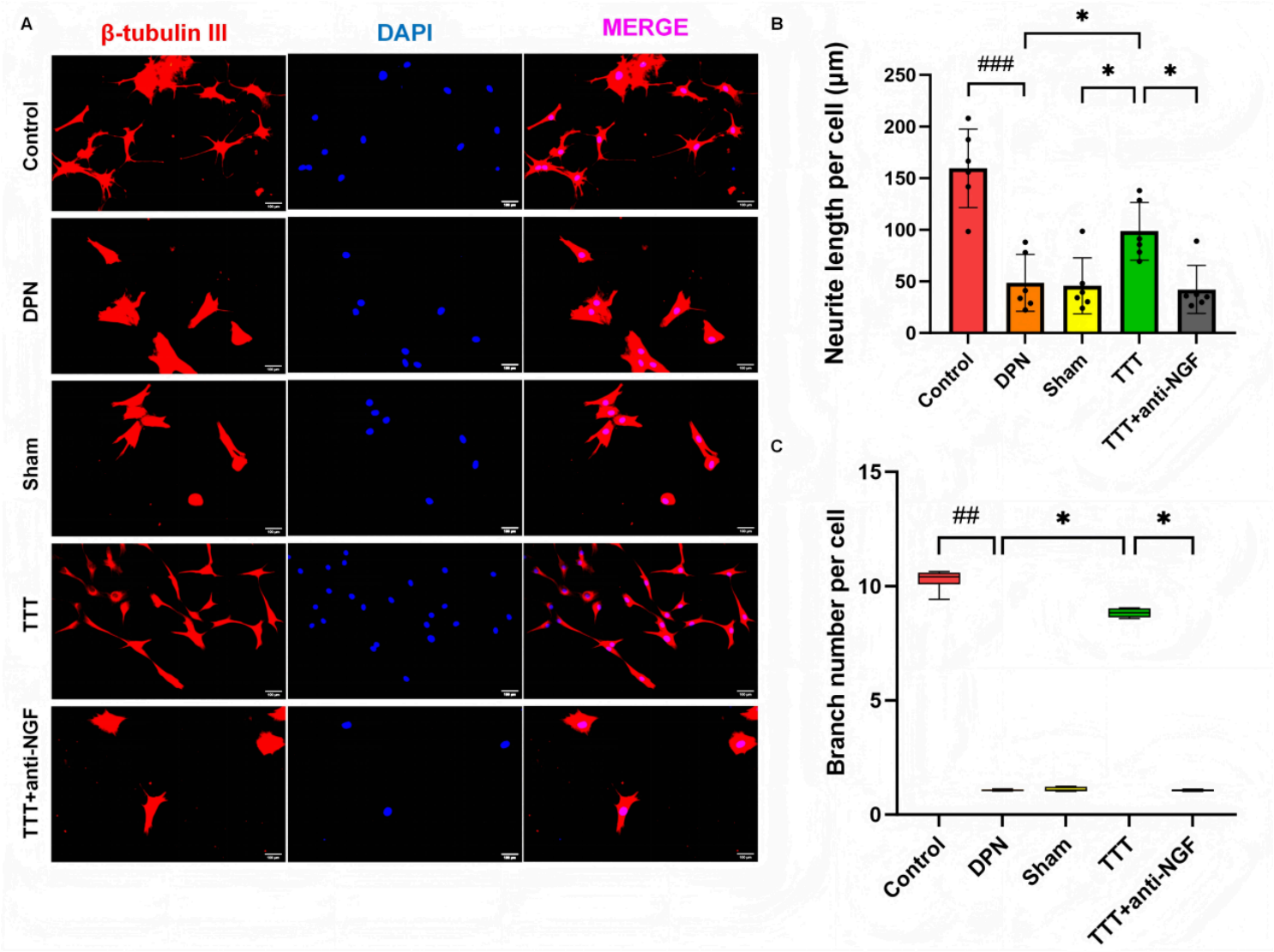


Figure 5

Serum-primed Schwann cells promote DRG neurite outgrowth in an NGF-dependent manner. (A) Representative β-tubulin III immunofluorescence images of DRG neurons in the lower chamber after Transwell co-culture with serum-treated RSC96 cells confined to the upper 0.4-μm insert (scale bar = 100 μm). (B) Quantification of neurite length and (C) branch points per neuron from β-tubulin III–positive DRG neurons. For serum-priming experiments, n indicates the number of serum donor rats (n = 6 per group). For each donor, 50 randomly selected β-tubulin III–positive neurons were analyzed and averaged to yield one value per donor. Neurite length was analyzed by one-way ANOVA with Tukey's multiple comparisons.

Branch points were analyzed by Kruskal–Wallis test with Dunn's multiple comparisons using a priori contrasts (DPN vs. TTT; TTT vs. TTT+anti-NGF).

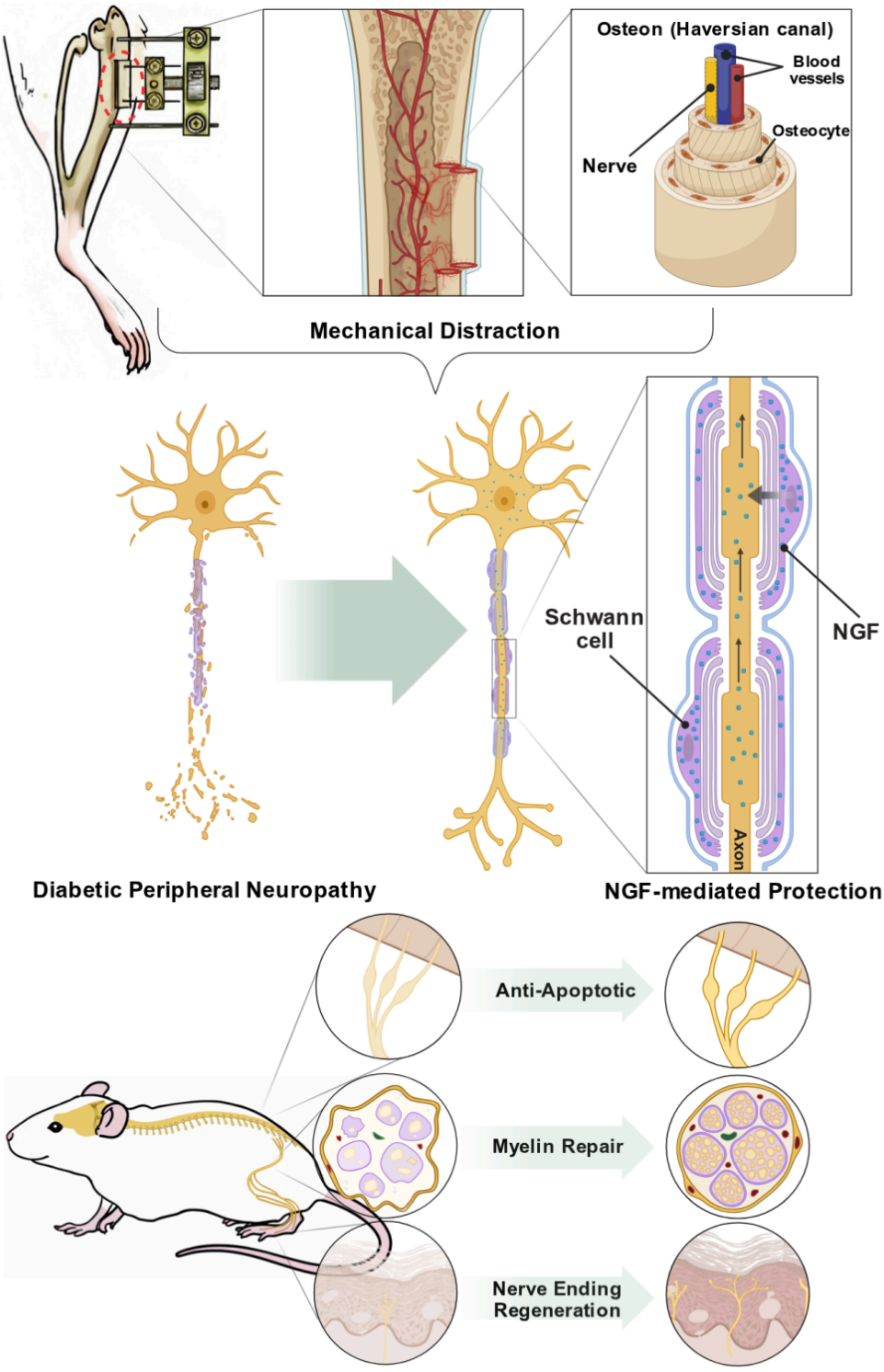


Figure 6

Proposed model for how tibial transverse transport (TTT) may ameliorate diabetic peripheral neuropathy (DPN). TTT-induced cyclic microstrain generated by tibial distraction is proposed to be transmitted through the periosteal surface and Haversian canal–embedded neurovascular pathways.

This mechanostimulation may modulate the perineural microenvironment and enhance NGF-related signaling in peripheral nerves, as supported by the modest increase of NGF detected in sciatic nerve lysates and the NGF-dependent effects observed in Schwann cell–based assays. Elevated local NGF signaling may promote neuronal and glial protection and support peripheral nerve structural and functional recovery, consistent with reduced apoptosis and improved intraepidermal nerve fiber–related signals in TTT-treated DPN rats. The DRG-related effects illustrated here represent inferred mechanisms based on in vitro co-culture results showing enhanced neurite outgrowth from DRG neurons stimulated by TTT-serum–primed Schwann cells. Items depicted as “myelin repair” and “nerve ending regeneration” indicate potential downstream outcomes and require further direct validation with myelin/axon-specific analyses.

Supplementary Files

This is a list of supplementary files associated with this preprint. Click to download.

- FigureS1caption.docx
- FigureS2caption.docx
- Graphicalabstract.png
- FigureS2.png
- FigureS1.png